Tellus (1983), *35A*, 241–255

Seasonal distributions of diabatic heating during the First GARP Global Experiment

By MING-YING WEI, *Space Science and Engineering Center*, DONALD R. JOHNSON, *Department of Meteorology, Space Science and Engineering Center and* RONALD D. TOWNSEND[1], *Department of Meteorology, University of Wisconsin-Madison, 1225 West Dayton Street, Madison, Wisconsin 53706, U.S.A.*

(Manuscript received April 27; in final form October 28, 1982)

ABSTRACT

The seasonal and annual global distributions of diabatic heating during the First GARP Global Experiment (FGGE) are estimated using the isentropic mass continuity equation. The data used are from the FGGE Level IIIa analyses generated by the United States National Meteorological Center. Spatially and temporally coherent diabatic heating distributions are obtained from the isentropic planetary scale mass circulation that is forced by large-scale heat sources and sinks.

The diabatic heating in the Northern Hemisphere is closely associated with the distribution of land and ocean. While cooling prevails over Eurasia and North America and heating occurs along the east coasts of these two continents during northern winter, a contrasting situation exists during northern summer with heating over most of the continents and cooling over the oceans where subtropical anticyclonic circulations prevail. Heating in the tropics, mostly from moist convection, has considerable longitudinal variations which change seasonally. Of particular importance is the seasonal progression of the primary centre of heating within the planetary scale Asiatic monsoon which is located over the western equatorial Pacific during northern winter and near the Philippines and Southeast China during northern summer.

1. Introduction

Estimates of large-scale diabatic heating have generally been determined by two different methods. One method is to independently estimate the individual components of radiational, condensational and sensible heating (e.g., Budyko, 1963; Newell et al., 1969, 1974). The other is to obtain the net heating from the energy balance required by the first law of thermodynamics (e.g., Hantel and Baader, 1978; Geller and Avery, 1978; Lau, 1979). In this study the results from an alternative method utilizing the mass continuity equation in isentropic coordinates (Johnson, 1980) will be presented and discussed.

The identification of large-scale heat sources and sinks of the atmosphere is basic to the study of thermally-forced general circulation. Within the isentropic framework, the planetary scale mass and energy transport can be directly linked to the distribution of heat sources and sinks (Johnson et al., 1981). The vertical mass transport is upward through isentropic surfaces in heat source regions and downward in heat sink regions; the horizontal mass transport is from heat source to heat sink in higher-valued isentropic layers and vice versa in lower-valued isentropic layers. The planetary scale transport of energy within the atmosphere is also intimately related to differential heating (Johnson and Townsend, 1981; Johnson et al., 1981). Net energy transport occurs through the condition that more energy is transported by the upper branch of the circulation from heat source to heat sink than is returned by the lower branch from heat sink to heat source. This article specifically addresses the three-dimensional analyses of heat sources and sinks and compares the results with those from earlier investigations.

The present study utilizes the FGGE (First

[1] Present affiliation: DET3 HQ Air Weather Service, Sunnyvale AFB, California, U.S.A.

GARP Global Experiment) Level IIIa data set generated by the United States National Meteorological Center for the period from December 1978 to November 1979. The objectives are to demonstrate the credibility of estimating diabatic heating rates from the observed isentropic mass circulation and to examine the global large-scale distributions of heat sources and sinks. A discussion of seasonal variation and annual distribution of net atmospheric heating is presented within which particular emphasis is placed on the Asiatic monsoon.

2. Method

The time-averaged equation of continuity in isentropic coordinates is given by

$$\frac{\partial}{\partial t_\theta}\overline{(\rho J_\theta)}^t + \nabla_\theta\cdot\overline{(\rho J_\theta \mathbb{V})}^t + \frac{\partial}{\partial\theta}\overline{(\rho J_\theta\dot{\theta})}^t = 0 \tag{1}$$

where ρ is density, θ is potential temperature, $\mathbb{V}$ is the horizontal wind velocity, J_θ is the transformation Jacobian ($|\partial h/\partial\theta|$), h is height and $\overline{(\ )}^t$ denotes the time average. With a vertical integration and the assumption that the vertical mass transport vanishes at the top of the atmosphere, the vertical mass flux through an isentropic surface is given by

$$\overline{(\rho J_\theta\dot{\theta})}^t = \int_\theta^{\theta_T}\left[\frac{\partial}{\partial t}\overline{(\rho J_\theta)}^t + \nabla_\theta\cdot\overline{(\rho J_\theta\mathbb{V})}^t\right]\mathrm{d}\theta \tag{2}$$

where θ_T represents the potential temperature at the top of the atmosphere. The three-dimensional distribution of diabatic heating can therefore be determined from the mass-weighted average of the vertical mass flux,

$$\langle\dot{\theta}\rangle^t = \frac{\overline{(\rho J_\theta\dot{\theta})}^t}{\overline{(\rho J_\theta)}^t} \tag{3}$$

Although the time-averaged diabatic mass flux in (2) is determined from the time-averaged mass circulations, it is evident that the instantaneous diabatic heating can be determined from an integration of the mass continuity equation without time averaging.

If an appropriate period of time is used such that the time-averaged mass distribution $\overline{(\rho J_\theta)}^t$ can be regarded as steady state, (1) reduces to

$$\nabla_\theta\cdot\overline{(\rho J_\theta\mathbb{V})}^t = -\frac{\partial}{\partial\theta}\overline{(\rho J_\theta\dot{\theta})}^t \tag{4}$$

Physically (4) states that, under the assumption of steady state, the divergence of the horizontal mass transport in an isentropic layer is directly coupled to the vertical derivative of the diabatic mass transport.

Two constraints on the time-averaged mass transport are implied from the steady state assumption. To isolate the first, let θ_{s_0} denote the lowest potential temperature that occurs at the surface during the time period considered. A vertical integration of (4) from θ_{s_0} to θ_T with the conditions that $\overline{(\rho J_\theta\dot{\theta})}^t$ vanishes at both boundaries of the time-averaged state yields

$$\int_{\theta_{s_0}}^{\theta_T}\nabla_\theta\cdot\overline{(\rho J_\theta\mathbb{V})}^t\,\mathrm{d}\theta = 0 \tag{5}$$

The upper boundary condition is satisfied from the fact that vertical mass flux vanishes at the top of the atmosphere while the lower one is imposed through the use of the Lorenz convention (Dutton and Johnson, 1967) that mass ρJ_θ is identically zero for all isentropes underground. This constraint requires that vertical integral of the quasi-horizontal isentropic mass transport be non-divergent. It also guarantees that the zonally and vertically integrated meridional mass transport across each latitude vanish.

The second constraint, revealed through an areal integration of (2) and use of the divergence theorem, is given by

$$\int\overline{(\rho J_\theta\dot{\theta})}^t\,\mathrm{d}A = 0 \tag{6}$$

The constraint requires that the upward diabatic mass transport through each isentropic surface be balanced by the downward mass transport and that the horizontal scales of planetary mass transport correspond to those of diabatic heating. For a simple two-layered structure of the atmosphere with a parabolic-type profile of vertical mass transport, the horizontal mass transport from heat source to heat sink above the level of maximum diabatic mass flux must be equal to the transport from heat sink to heat source below the maximum level.

In these analyses it should be recognized that the distribution of diabatic heating is determined from the equation of mass continuity and thus is directly related to the mass circulation as viewed in isentropic coordinates. This strategy is fundamentally different from the indirect method of estimating diabatic heating in the first law of thermodynamics as a residual term from the balance of energy. The vertical mass flux defined in (2) corresponds to the diabatic portion of the vertical motion conventionally defined for isobaric or Cartesian coordinates. Under adiabatic and inviscid conditions, a flow is simply two-dimensional in the isentropic framework whereas in other coordinate systems the embedded adiabatic vertical motion requires that the flow be three-dimensional. Consequently, the horizontal and vertical length scales of mass circulation in other coordinate systems bear no direct relation to the distribution of heating.

The feasibility of using the isentropic equation of continuity rests upon the condition that planetary scale differential heating determines both the direction and the horizontal scales of a systematic global mass circulation within the structure of the atmosphere. Over time scales within which the average mass distribution is steady, the heating distribution is directly inferred from the mass transport. In contrast, the heating distribution determined through an isobaric analysis of the thermodynamic energy equation involves a fine state of balance between energy transport processes of relatively large magnitudes and opposite signs.

A complete discussion of the differences in the above methods is beyond the purpose of this paper. However, it is helpful to consider the following two vector relations between transport processes in isentropic and isobaric coordinates. The divergence of the mass and enthalpy transport in isentropic coordinates may be expressed by:

$$\nabla_\theta \cdot (\rho J_\theta \mathbb{V}) = \rho J_\theta \left\{ \nabla_p \cdot \mathbb{V} - \frac{\partial}{\partial p} \left(\frac{\partial p}{\partial \theta} \mathbb{V} \cdot \nabla_p \theta \right) \right\}$$

$$\nabla_\theta \cdot (\rho J_\theta \mathbb{V} c_p T) = \rho J_\theta \left\{ \nabla_p \cdot (\mathbb{V} c_p T) - \frac{\partial}{\partial p} \left(c_p T \frac{\partial p}{\partial \theta} \mathbb{V} \cdot \nabla_p \theta \right) \right\}$$

Note, first of all that the isobaric determination of diabatic heating involves analysis of transport processes using the second equation while the isentropic determination involves analysis of transport processes using the first equation. Dimensionally and physically these two equations measure different processes. The divergent mode of quasi-horizontal mass transport in isentropic coordinates, in contrast to isobaric or Cartesian coordinates, includes both the geostrophic and ageostrophic components which allow for the unconstrained exchange of mass between tropical and polar latitudes. The geostrophic component, resulting from the covariance between mass ρJ_θ and the geostrophic velocity (Johnson and Downey, 1975; Johnson, 1979), contributes through the horizontal advection of mass within an isentropic layer. Within amplifying baroclinic waves, a net poleward transport of subtropical air masses in warmer isentropic layers and equatorward transport of polar air in colder isentropic layers provides the structure for this systematic covariance. Within the isobaric framework this is a degree of freedom that is confined to the thermodynamic equation. The isobaric mass circulations, being restricted to scales of imbalances essentially defined through ageostrophic motion, cannot serve to transport energy from a heat source to a heat sink at the planetary scale. Consequently an isobaric determination of the heating distribution through the first law of thermodynamics involves calculation of a fine state of balance between adiabatic and diabatic modes of heating associated with dp/dt and between geostrophic and ageostrophic modes of energy transport associated with horizontal motion. At this point in time, any definitive conclusions concerning the relative accuracy or advantages of one method over the other remain to be determined.

3. Data and numerical procedure

The FGGE Level IIIa data set, obtained from the National Center for Atmospheric Research, was generated operationally by the United States National Meteorological Center (NMC) using an optimum interpolation scheme (Bergman, 1979; McPherson et al., 1979). Global distributions of geopotential height, temperature, zonal and meridional wind components, valid at 00.00 and 12.00 GMT for the period from December 1, 1978 to November 30, 1979, were available at a 2.5° latitude–longitude grid for each of the twelve mandatory pressure levels from 1000 to 50 mb.

The first step in the calculations was to convert data from isobaric to isentropic coordinates. For this conversion, knowledge of the earth's surface temperature is desired. Unfortunately, during certain periods of the FGGE year the surface temperatures within NMC's FGGE Level IIIa data set were not consistently updated. Since the temperatures at the mandatory pressure levels were originally interpolated from sigma coordinates, the temperatures at the earth's surface were approximated at each grid point by a linear interpolation of temperature with geopotential height (Townsend, 1980). Subjective evaluation shows that the surface temperatures so created are satisfactory for large-scale diagnostics. A linear interpolation of pressure and all other parameters with $\theta^{1/\kappa}$ was used in converting the isobaric data to global isentropic analyses at 16 levels with 10 K vertical resolution. For the time-averaged circulation, the minimum isentropic surface is determined by the lowest potential temperature observed at the surface within the global domain. Whenever an isentropic surface goes "underground", surface values of pressure are assigned (Lorenz, 1955). In all cases the potential temperature at the top level is equal to or greater than 370 K and the pressure is generally less than 180 mb. Therefore nearly all of the tropospheric circulation is included. More details on data processing are presented by Townsend (1980).

The horizontal grid resolution used in this study is 5° in both latitude and longitude directions. Although data are available in 2.5° resolution, a comparison between 2.5° and 5° revealed that results from 5° resolution retain the primary features of the large-scale circulation. Thus, the 5° resolution was utilized due to the more economical aspects.

Analysis of the quasi-steady assumption used in the last section verified that the local time rate of change of mass is at least one order of magnitude smaller than the horizontal divergence of mass transport for the time span being considered, i.e., a season or a year. Under the quasi-steady state assumption, one essential requirement for successful estimates of diabatic mass flux is that the vertically integrated mass divergence vanish (Holopainen, 1965). In most cases, due to truncation errors, such a balance is not satisfied in the computations; thus a mass-weighted adjustment is made according to

$$\int_{\theta_{s_0}}^{\theta_T} \left[\nabla_\theta \cdot \overline{(\rho J_\theta \mathbb{V})}^t - \int_{\theta_{s_0}}^{\theta_T} \nabla_\theta \cdot \overline{(\rho J_\theta \mathbb{V})}^t \, d\theta \; \frac{(\overline{\rho J_\theta})^t}{\int_{\theta_{s_0}}^{\theta_T} (\overline{\rho J_\theta})^t \, d\theta} \right] d\theta = 0 \tag{7}$$

For the periods considered, the average adjustment is generally within 20% of the maximum mass divergence of the original profile and the regional distribution of divergence and convergence is essentially unchanged.

For the purpose of examining large-scale diabatic processes, two filtering techniques are applied to fields of quasi-horizontal mass divergence. Zonal harmonics with wavelength less than 4000 km are first deleted through truncation of one-dimensional Fourier transforms. The percentage of variance retained in the mass divergence during December 1978–February 1979 after the Fourier filtering is presented in Table 1. Spatial smoothing is then accomplished by applying a low pass filter and an inverse filter in both east–west and north–south directions (Holloway, 1958). The low pass filter has weights (1, 2, 1) and the inverse filter (−1, 5, −1). The response of this combination is roughly 50% for a wavelength of five grid increments. A comparison of the mass divergence without and with filtering and smoothing for the 300–310 K isentropic layer during December 1978–February 1979 is presented in Fig. 1. The distribution and intensity of diabatic heating estimated with filtering seems agreeable with climatological concepts and indicates that the large-scale information is unaltered.

4. Results

Seasonal averages of global diabatic heating rates during the FGGE year are computed for the four periods: December 1978–February 1979, March–May, June–August and September–November, 1979, respectively. The results will be presented by mass-weighted averages in three formats:

(i) Horizontal distributions of vertically averaged diabatic heating defined by

$$\langle \dot{\theta} \rangle^{\theta,t} = \frac{\overline{(\rho J_\theta \dot{\theta})}^{\theta,t}}{(\overline{\rho J_\theta})^{\theta,t}} \tag{8}$$

(ii) Meridional cross-sections of zonally averaged diabatic heating defined by

$$\langle \dot{\theta} \rangle^{\lambda,t} = \frac{\overline{(\rho J_\theta \dot{\theta})}^{\lambda,t}}{(\overline{\rho J_\theta})^{\lambda,t}} \tag{9}$$

Table 1. *Percentage of variance retained in the mass divergence during December 1978–February 1979 when zonal Fourier filtering is applied with a cut-off at 4000 km. The potential temperature indicates the bottom of a 10 K layer*

	Potential temperature														
Latitude	220	230	240	250	260	270	280	290	300	310	320	330	340	350	360
90	0.0	0.0	0.0	0.0	0.0	0.0	0.0	0.0	0.0	0.0	0.0	0.0	0.0	0.0	0.0
85	0.0	0.0	0.0	0.0	0.0	0.0	0.0	0.0	0.0	0.0	0.0	0.0	0.0	0.0	0.0
80	0.8	12.5	23.5	31.9	11.0	10.8	8.2	1.2	1.5	10.5	4.4	9.9	23.3	18.1	5.0
75	20.8	14.3	18.5	35.6	13.8	38.4	1.6	10.1	16.5	22.8	30.6	18.6	22.5	22.3	7.5
70	4.1	22.0	35.6	61.3	42.4	27.9	12.3	30.3	11.3	27.9	3.9	7.0	17.0	17.5	15.8
65	12.3	29.2	42.2	62.6	57.1	12.7	34.7	19.4	10.8	21.8	16.3	11.0	24.3	34.2	9.1
60	30.1	12.0	35.0	46.3	51.2	48.3	40.9	16.8	56.5	29.4	19.5	32.8	41.6	47.0	45.6
55	0.0	30.1	44.2	35.9	32.4	37.2	46.1	28.8	34.5	31.1	9.9	39.2	20.7	26.6	51.6
50	0.0	73.1	61.7	53.9	60.1	42.4	36.7	36.8	25.0	54.1	37.6	37.1	41.1	60.2	73.6
45	0.0	72.0	81.1	64.6	83.7	61.9	42.3	47.6	28.2	44.0	44.1	39.4	39.5	61.0	44.4
40	0.0	0.0	56.0	81.9	84.6	64.3	60.7	58.8	24.5	54.0	37.6	46.7	23.7	39.6	43.4
35	0.0	0.0	0.0	67.0	84.8	67.9	61.9	44.6	44.2	51.7	33.5	53.6	56.7	39.3	63.8
30	0.0	0.0	0.0	48.1	71.2	83.2	54.4	44.4	49.6	34.6	59.7	47.9	55.6	61.9	63.0
25	0.0	0.0	0.0	0.0	61.6	65.7	62.9	23.2	47.8	39.8	23.6	53.1	40.2	42.3	43.1
20	0.0	0.0	0.0	0.0	0.0	54.9	59.7	48.9	38.5	41.4	40.2	51.5	34.9	57.4	51.1
15	0.0	0.0	0.0	0.0	0.0	0.0	59.6	58.1	62.9	56.2	39.8	51.6	51.8	28.2	31.9
10	0.0	0.0	0.0	0.0	0.0	0.0	64.5	79.6	49.6	51.4	60.5	46.2	63.9	54.2	69.9
5	0.0	0.0	0.0	0.0	0.0	0.0	28.5	52.8	58.9	69.1	69.9	72.6	72.1	59.2	74.9
0	0.0	0.0	0.0	0.0	0.0	0.0	31.6	69.0	78.0	63.6	80.0	82.3	70.1	72.0	71.7
−5	0.0	0.0	0.0	0.0	0.0	0.0	16.3	66.4	70.8	62.7	63.2	62.3	71.1	64.2	66.8
−10	0.0	0.0	0.0	0.0	0.0	0.0	39.6	61.2	84.5	50.6	44.6	62.8	73.4	79.1	85.5
−15	0.0	0.0	0.0	0.0	0.0	0.0	57.1	70.1	78.3	66.4	37.2	65.8	80.0	82.9	78.7
−20	0.0	0.0	0.0	0.0	0.0	38.8	52.1	75.8	75.6	48.7	52.7	52.8	66.1	61.8	73.7
−25	0.0	0.0	0.0	0.0	0.0	32.8	61.9	74.8	53.3	68.5	42.3	55.1	59.1	52.0	54.8
−30	0.0	0.0	0.0	0.0	0.0	17.0	36.7	68.5	37.3	48.3	23.8	33.0	36.6	50.7	71.4
−35	0.0	0.0	0.0	0.0	0.0	22.8	39.3	69.7	34.7	55.4	55.6	71.5	68.1	68.2	72.3
−40	0.0	0.0	0.0	0.0	0.0	57.1	45.0	29.9	43.0	34.2	41.9	50.6	58.9	59.4	43.4
−45	0.0	0.0	0.0	0.0	13.9	38.2	32.0	30.7	50.0	23.4	51.0	38.3	42.6	33.3	39.1
−50	0.0	0.0	0.0	0.0	10.9	34.6	42.4	43.3	55.3	36.0	53.9	52.0	62.8	51.9	56.6
−55	0.0	0.0	0.0	0.0	6.2	44.3	43.0	39.2	28.2	33.9	45.9	61.2	52.6	45.6	48.7
−60	0.0	0.0	0.0	2.7	23.4	69.0	41.0	32.2	53.6	52.1	29.3	28.1	33.5	40.8	33.9
−65	0.0	0.0	0.0	27.1	69.6	67.4	30.5	63.3	68.0	21.5	27.9	26.5	33.2	30.5	30.3
−70	0.0	0.0	0.0	22.8	30.3	14.4	37.0	8.5	36.5	30.7	36.5	21.7	15.8	9.7	10.7
−75	0.0	0.0	0.0	26.9	51.1	32.7	9.6	37.4	37.4	11.3	5.7	25.4	19.4	27.2	26.6
−80	0.0	0.0	0.0	5.7	16.8	14.4	15.8	17.2	17.4	7.2	9.9	2.0	2.2	2.9	2.3
−85	0.0	0.0	0.0	0.0	0.0	0.0	0.0	0.0	0.0	0.0	0.0	0.0	0.0	0.0	0.0
−90	0.0	0.0	0.0	0.0	0.0	0.0	0.0	0.0	0.0	0.0	0.0	0.0	0.0	0.0	0.0

(iii) Meridional profiles of zonally and vertically averaged diabatic heating defined by

$$\langle \dot{\theta} \rangle^{\lambda,\theta,t} = \frac{\overline{(\rho J_\theta \dot{\theta})}^{\lambda,\theta,t}}{\overline{(\rho J_\theta)}^{\lambda,\theta,t}} \qquad (10)$$

where

$$\overline{(\;)}^t = \frac{1}{t_n - t_0} \int_{t_0}^{t_n} (\;)\,\mathrm{d}t$$

$$\overline{(\;)}^\theta = \frac{1}{\theta_T - \theta_{s_0}} \int_{\theta_{s_0}}^{\theta_T} (\;)\,\mathrm{d}\theta$$

$$\overline{(\;)}^\lambda = \frac{1}{2\pi} \int_0^{2\pi} (\;)\,\mathrm{d}\lambda.$$

Note that $\langle \dot{\theta} \rangle^t$ is an estimate of net diabatic processes in the atmosphere. No distinction between radiational, sensible, and latent heating can

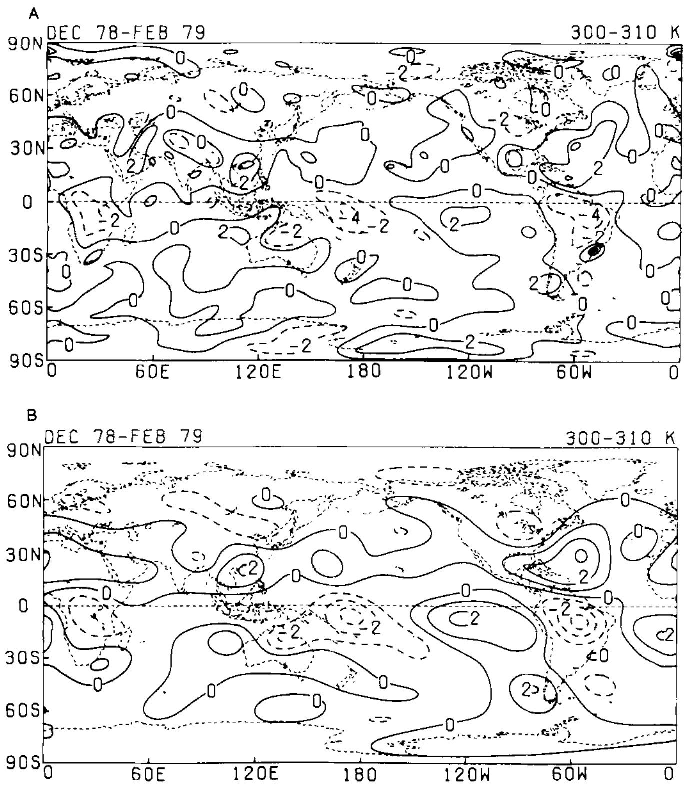

Fig. 1. Quasi-horizontal mass divergence (10^{-4} kg m^{-2} s^{-1} K^{-1}) in the 300–310 K isentropic layer for December 1978–January 1979 (a) without and (b) with filtering (see text).

explicitly be determined through this approach. Inferences as to the particular component or components that dominate in a particular region must be based on physical and climatological insight.

4.1 *Horizontal distributions of vertically averaged diabatic heating*

Horizontal distributions of vertically averaged diabatic heating for the four seasons during the FGGE year are shown in Fig. 2. The most notable features in all four seasonal distributions are the heating contrasts associated with land and ocean, the subtropical anticyclonic and mid-latitude cyclonic circulations, and the persistence of the Asiatic monsoon. The Asiatic monsoon refers to the seasonally varying regimes of the planetary scale circulation in the Eastern Hemisphere which extends in latitude from the southern oceans of the Southern Hemisphere to the northern reaches of Eurasia and in longitude across Africa to the west and the Pacific Ocean to the east (Webster et al., 1977).

In December 1978–February 1979 (Fig. 2a), the Asiatic monsoon has an extensive area of heating with maximum in excess of 1.5 K day^{-1} located to the east of New Guinea. The upward mass flux in this area and the downward mass flux over the eastern Pacific where cooling is observed correspond, respectively, to the upward and downward branches of a Walker-type circulation in the isentropic framework (Johnson and Townsend, 1981).

It has been indicated that the 1978–79 winter monsoon is relatively weak (e.g., Tanaka, 1981). The time-averaged heating maximum just to the east of New Guinea is consistent with Tanaka's (1981) findings that only one ITCZ (intertropical convergence zone) is observed near New Guinea during weak monsoon years in contrast to two ITCZs when the monsoon is strong.

Another prominent area of heating with a maximum of 1.5 K day^{-1} is nicely outlined over

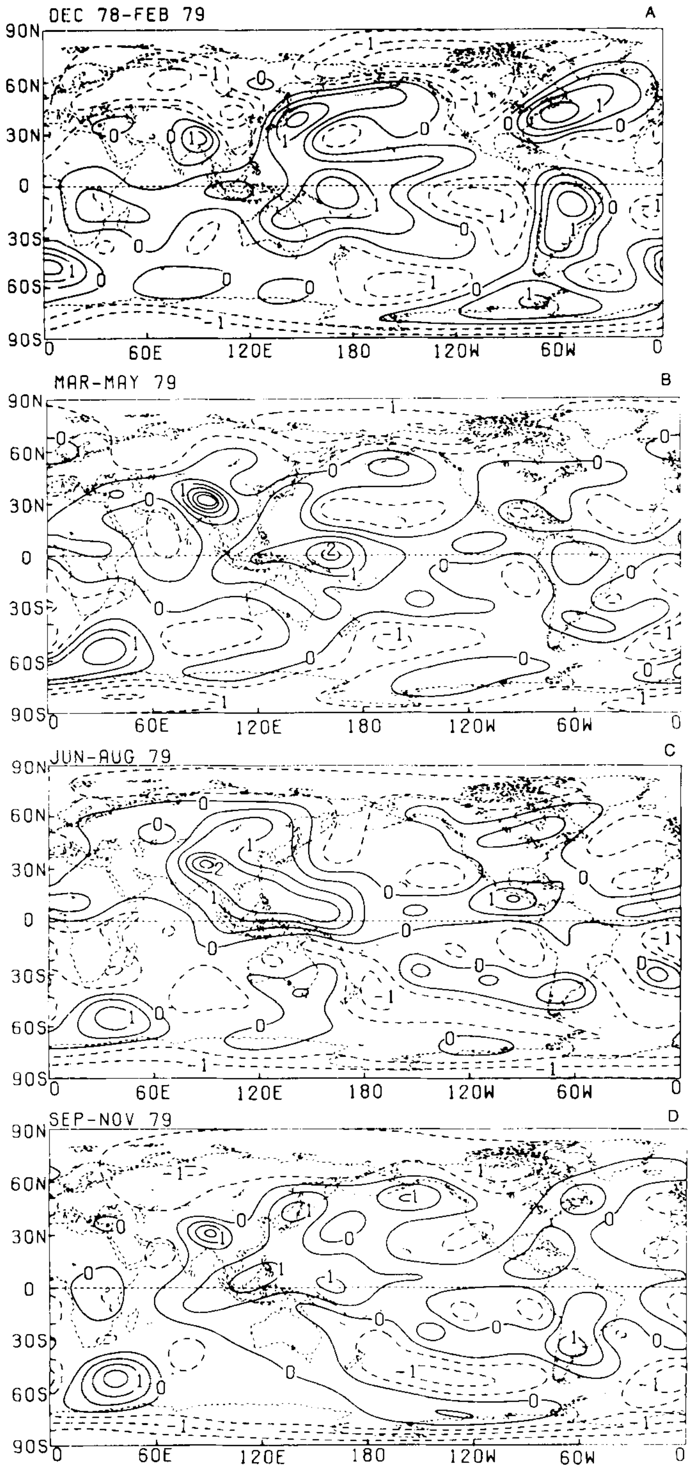

Fig. 2. Mass-weighted vertically averaged diabatic heating rates (K day^{-1}) for the four seasons of the FGGE year.

South America. Daily convection in this region can be easily identified from the GOES-East infrared imagery, especially during the Special Observing Period I (January 13–February 13, 1979). Other areas of heating in the tropics include the southeast part of Africa and central Indian Ocean. They correspond well with regions of large mean cloud cover (Atkinson and Sadler, 1970; Miller and Feddes, 1971).

In the middle lattitudes of the Northern Hemisphere, large heating occurs along the cyclone tracks to the east coasts of Asia and North America. The source of energy must come from both the sensible heating from the ocean and the latent heat release within the atmosphere. For this particular northern winter, the diabatic heating associated with the cyclogenesis along the American coast appears to be stronger than that along the Asian coast. The winter season of the FGGE year was exceptionally severe over North America in association with frequent and intense outbreaks of cold continental polar air masses which moved eastward over the relatively warm Gulf Stream. Net cooling prevails over both the North American and Eurasian continents, as well as the Sahara Desert. Cooling rates exceeding 1 K day^{-1} are evident in the source regions of continental polar air masses over Canada, Alaska, Siberia and Mongolia.

The interpretation of the heating distribution in the mid and high latitudes of the Southern Hemisphere is somewhat restricted due to less distinct synoptic patterns associated with land and ocean and more uncertainties in the data. Heating is shown over Australia, ranging from 1 K day^{-1} in the northeast to zero in the south and west. However, this distribution is uncertain since climatologically most of Australia is under the influence of heat lows during southern summer except for the northern and eastern coasts where a significant amount of rainfall is received (Taljaard, 1967; Year Book Australia, 1981). Using satellite mosaic sequences during the southern summer months of 1966–69, Streten and Troup (1973) found that the formation and movement of cyclonic circulations are suggestive of a high frequency of a basic three long wave pattern around the hemisphere. Such a pattern displays cyclogenesis east of South America associated with cyclolysis near Enderby Land and further east; cyclogenesis from Kerguelen to southern Australia and cyclosis near Adelie Land and the Ross Sea; and cyclogenesis in the central South Pacific with cyclolysis in the Bellinghausen Sea. Some features in the heating distribution determined here during FGGE correspond with the results of Streten and Troup (1973); however, the similarity is not well defined. The band of heating stretching southeastward from New Guinea corresponds with high mean cloud cover associated with disturbances originating in subtropical latitudes that move southeastward toward the circumpolar vortex (Miller and Feddes, 1971). The cooling indicated over the oceans southeast of New Zealand appears realistic due to the relatively frequent anticyclonic circulations in the area (Hill, 1981). More information with regard to the synoptic patterns and mean cloud distributions during FGGE are needed in order to assess the representativeness of the heating distribution in the Southern Hemisphere.

The heating distribution for March–May 1979 (Fig. 2b) shows that the primary center of maximum heating of the Asiatic monsoon has moved northwestward to a location over the equator. A secondary center of maximum heating is located over the Tibetan Plateau. Tropical deep convection appears to be active along the equator in the Pacific. However, the convection over South America has decreased in intensity, as well as the heating along the two cyclone tracks in the Northern Hemisphere. Note how net heating begins to extend into the interior of the continents. Regions of net cooling occur in the subtropical anticyclonic circulations over the Pacific and Atlantic Oceans in both hemispheres.

As the march of the seasons continues into northern summer (Fig. 2c), the contrast between land and ocean becomes apparent. Net heating reaches as far north as 60° N over the Asian and American continents. Net cooling dominates the polar region. With the intensification of the subtropical anticyclones in the Northern Hemisphere, the areal expanse of net cooling in the North Pacific and Atlantic is more extensive, especially in the eastern halves. The ITCZ, now situated mostly north of the equator, meanders around the globe. The Asiatic monsoon assumes its northernmost position with maximum heating over the Philippines and Tibet. The heating rate associated with moist convection over Central America exceeds 1 K day^{-1}. The Sahel region of Africa receives net heating since June–August is the rainy season for this area. Heating is also indicated over portions of the Sahara and Arabian deserts. Possible contributing factors are increased shortwave absorption due to presence of dust (Carlson and Benjamin, 1980) and large sensible heat transfer from the surface to the atmosphere (Cox and Ackerman, 1981).

Major cyclogenesis regions in the Southern Hemisphere during the southern winter of 1979 are located southeast of Africa and south of Australia at about 55° S, as well as in the mid-Pacific Ocean and to the lee of the Andes near 45° S (Physick, 1981). The former two lie in a belt of upper level zonal wind maxima in the Indian Ocean around 50° S and the latter two lie downstream and poleward of a subtropical jet in the South Pacific near 25–30° S. The heating indicated to the south of Africa and Australia, in mid-South Pacific and over southern South America are presumably associated with the latent heat release within extratropical cyclones that occur relatively frequently in these areas. The heating south of Africa reaches 1 K day^{-1}; however, the values in the other two areas are generally less than 0.5 K day^{-1}. Net cooling is indicated over most of the southern oceans. The extensive region of net cooling located to the east-southeast of New Zealand over the South Pacific Ocean is associated with relatively frequent anticyclones noted earlier. This region lies between a high latitude storm track that more or less circumscribes the Antarctic continent and the storm track associated with the subtropical jet (Hill, personal communication).

During the period from September to November 1979 (Fig. 2d), the distributions of diabatic processes appear to be intermediate between the summer and winter conditions. The heating over both the Asiatic monsoon region and central America decreases in intensity. The average position of the primary region of heating within the Asiatic monsoon has a slight southeastward shift. The heating over central America decreases while over the southern portion of Africa the heating increases. As the cooling in the north polar regions expands southward into the Asian and North American continents, the heating due to air–sea interaction and latent heat release resumes over the oceanic regions east of the two continents. Except for small relative changes in the intensity in the Southern Hemisphere, areal distribution of heating and cooling during September–November 1979 is remarkably similar to that during June–August 1979.

The results for the four seasons establish that the region of heating stretching from the Indian Ocean to the central Pacific and generally centered near the equator within the Asiatic monsoon is a persistent source of energy on the planetary scale. During December 1978 through February 1979 the region of heating is centered just east of New Guinea. As the season progresses, this region moves northwestward and joins with the Indian summer monsoon during June through August. Later the region retreats southeastward, thus completing a yearly cycle in its movement. Diabatic heating is strongest during June and August, a period when the Indian summer monsoon is active. Also noteworthy is the cooling within the subtropical anticyclone over the eastern equatorial Pacific which exists throughout the year; the cooling rate is largest during December to February. Although the diabatic heating within the Asiatic monsoon is most intense during June to August, the diabatic contrast between the western and eastern equatorial Pacific appears to be largest during December to February.

4.2. *Meridional cross-sections of zonally averaged diabatic heating*

Meridional cross-sections of zonally averaged diabatic heating within isentropic coordinates are shown in Fig. 3. During December to February 1979, net heating exists throughout the tropical troposphere extending approximately from 5° N to 30° S. This undoubtedly is associated with an excess of heating due to moist convection in the intertropical convergence zone and the Asiatic monsoon region over the radiational cooling occurring in oceanic anticyclones. A maximum of 0.55 K day^{-1} is located near the equator in the 310–320 K isentropic layer (not shown). The middle latitudes in the Northern Hemisphere are characterized by strong heating in lower isentropic layers and cooling in upper layers. The heating must be attributed to the sensible and latent energy added within the baroclinic disturbances which are strongest and most frequent during northern winter. A maximum exceeding 2.0 K day^{-1} appears near 30–40° N. With the exception of the region north of 80° N in the upper isentropic layers, the polar latitudes in the Northern Hemisphere are

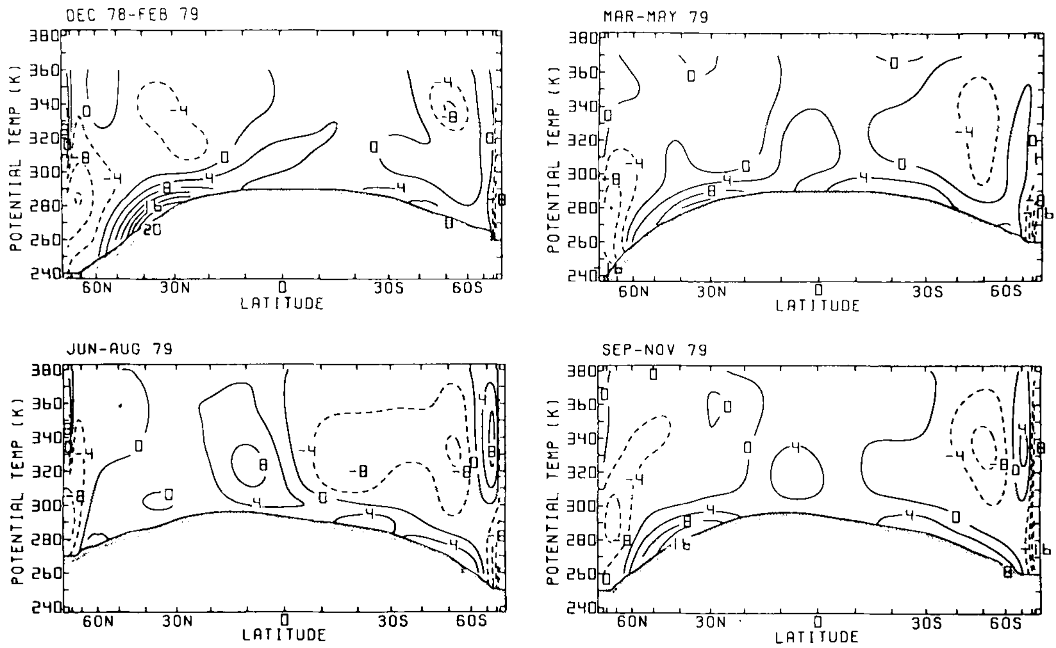

Fig. 3. Meridional cross-sections of mass-weighted zonally averaged diabatic heating rates (10^{-1} K day^{-1}). The shaded lines represent the earth's surface.

dominated by net cooling. The heating north of 80° N is not considered to be realistic and is probably due to the inadequacy of the data and numerical truncation near the pole. The largest cooling rate, greater than 1 K day^{-1}, occurs near 65–75° N in the 280–300 K isentropic layer. Similar features are shown for the Southern Hemisphere; however, the contrast between heating and cooling is less.

The distribution of diabatic processes described above, i.e., heating in the tropics and lower troposphere of middle latitudes as well as cooling in the polar regions and upper troposphere of middle latitudes, although modulated by seasonal variations, is a basic pattern for the entire year. The heating associated with the intertropical convergence zone is strongest during June–August 1979 and assumes its northernmost position. The maximum heating rate occurs in the 320–330 K layer near 10° N. The intense contrast between heating in lower isentropic layers and cooling in upper layers in the middle latitudes during northern winter is replaced with a moderate amount of heating in a large portion of the atmosphere during June–August 1979. During this same season, most of the troposphere in the southern subtropics and middle latitudes is dominated by cooling in excess of 0.4 K day^{-1} with the largest being greater than 0.8 K day^{-1}. Net heating occurs near the earth's surface at all latitudes except in polar regions.

4.3. *Meridional profiles of zonally and vertically averaged diabatic heating*

Meridional profiles of zonally and vertically averaged total diabatic heating are presented in Fig. 4. Meridional profiles derived from the quasi-horizontal mass divergence without any spatial smoothing are also plotted for reference. Notice that smoothing reduces the magnitude of extrema. The discussion focuses on results determined from spatial smoothing.

The profiles displayed primarily reflect the latitudinal distribution and seasonal variation of diabatic processes described earlier. The maximum heating in the tropics is roughly 0.8 K day^{-1} at 10° N during June to August 1979. The four-belt structure where the tropics and middle latitudes are characterized by net heating and the subtropics and very high latitudes by net cooling is clearly shown in the Northern Hemisphere during December 1978–February 1979. The decrease in cooling north of 80° N is a result of the questionable

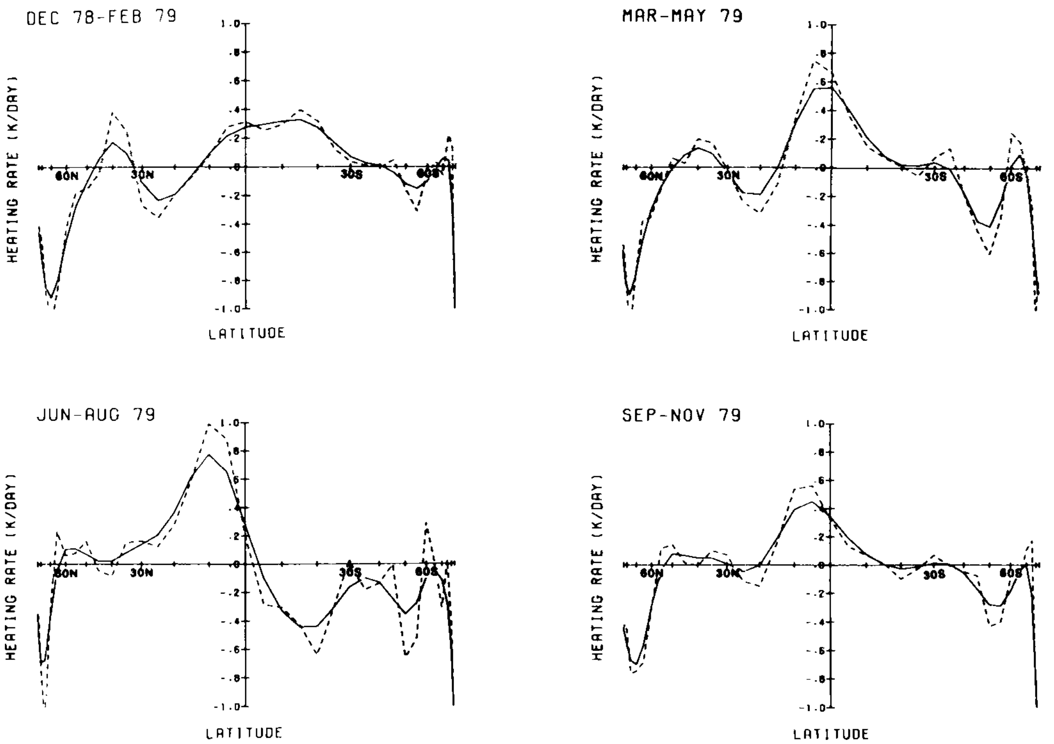

Fig. 4. Meridional profiles of the zonally and vertically averaged diabatic heating rates (K day^{-1}). The solid and dashed lines represent the distributions with and without filtering, respectively.

heating in upper isentropic layers noted earlier. The net heating resulting from baroclinic circulations in northern middle latitudes is prominent in the northern winter. However, in the Southern Hemisphere this feature is only reflected as a reduction of net cooling in mid-latitudes during southern winter. The decrease in heating is probably due to reduced sensible and latent heat flux from the ocean to cold polar air masses because of the lack of pronounced contrast between land and ocean in this maritime hemisphere. For both hemispheres the subtropics experience strong net cooling during the local winter season and net heating during local summer.

5. Comparisons

An analysis of the annual mean diabatic heating distribution for the atmosphere is presented in Budyko (1963). This analysis was prepared by summing up the components of radiation, condensation and boundary layer heating. For a comparison with Budyko's analysis, the vertical mass flux is computed for the annually averaged atmosphere during the FGGE year and then converted to an energy flux quantity according to

$$\overline{\int \rho Q \,\mathrm{d}z'} \simeq (c_p/p_{00}^{\kappa}) \int \overline{\rho J_\theta{}'} \langle \dot\theta \rangle' \langle p^{\kappa} \rangle' \mathrm{d}\theta \qquad (12)$$

where Q is rate of heat addition per unit mass. The approximation in (12) omits a term involving $\langle \dot\theta^{*} p^{\kappa *} \rangle'$ that arises with a temporal correlation between heating and the pressure level where heating occurs. Results for January 1979 indicate that this term is more than one order of magnitude smaller than the standing term. Thus, the omission of the transient term does not affect the heating distribution significantly.

In Fig. 5 the annual diabatic heating calculated from (12) (upper diagram) is compared with Budyko's diagram (lower). Considering the difference in methodology and data source, the similarities between the two, particularly in the

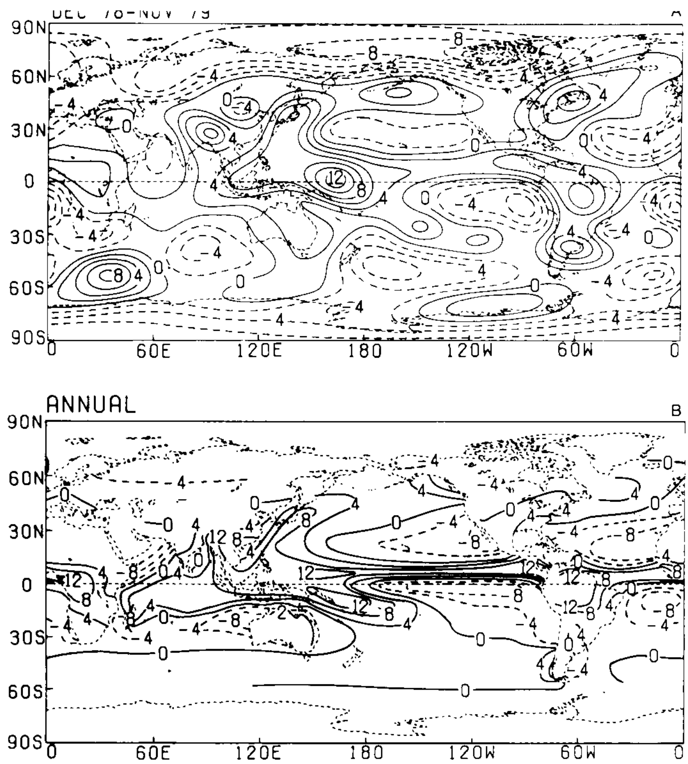

Fig. 5. Vertically averaged annual diabatic heating rates (10 W m^{-2}) (a) during the FGGE year and (b) adapted from Budyko (1963).

tropics and Northern Hemisphere, are striking. Some of the similarities include heating over central Africa, equatorial Indian Ocean and the East Indies. Large heating exists over the western equatorial Pacific with two branches stretching eastward into the North and South Pacific and then connecting with heating over South America and the equatorial Atlantic. Net heating is also shown in both figures in the eastern portion and coastal regions of Asia and North America. Cooling prevails over the polar latitudes, the interior of continents and the eastern portion of the North and South Pacific and Atlantic. The intensities of heating and cooling over most regions are quite comparable. However, the heating over South America and cooling over oceanic regions are one to two times larger in Budyko's results. Except for polar latitudes where no comparison can be made due to lack of information in Budyko's results, the most notable difference between the two figures occurs over Australia and in the southern oceans of the Southern Hemisphere. In the result from FGGE, a gradual decrease in heating is indicated from the northeast of Australia to the southwest; also indicated is the large zonal asymmetry in the heating distribution in the southern oceans. However, in Budyko's results, maximum heating in Australia occurs along most of the coastal areas and a zonal band of heating exists near 40–60° S. Further investigation and a better knowledge of the distribution of high-latitude cyclones in the Southern Hemisphere are needed to reconcile these differences.

Based on Budyko's (1963) atlas and London's (1957) radiational cooling estimates north of 60° N, Holopainen (1965) computed the zonally averaged diabatic heating for the Northern Hemisphere, shown in Fig. 6b. The four-belt structure in the Northern Hemisphere is evident in both the FGGE (Fig. 6a) and Holopainen's distributions. However, the heating in the tropics is more intense in Holopainen's result.

The intensities of the tropical Hadley cells in the isobaric mean meridional circulations determined

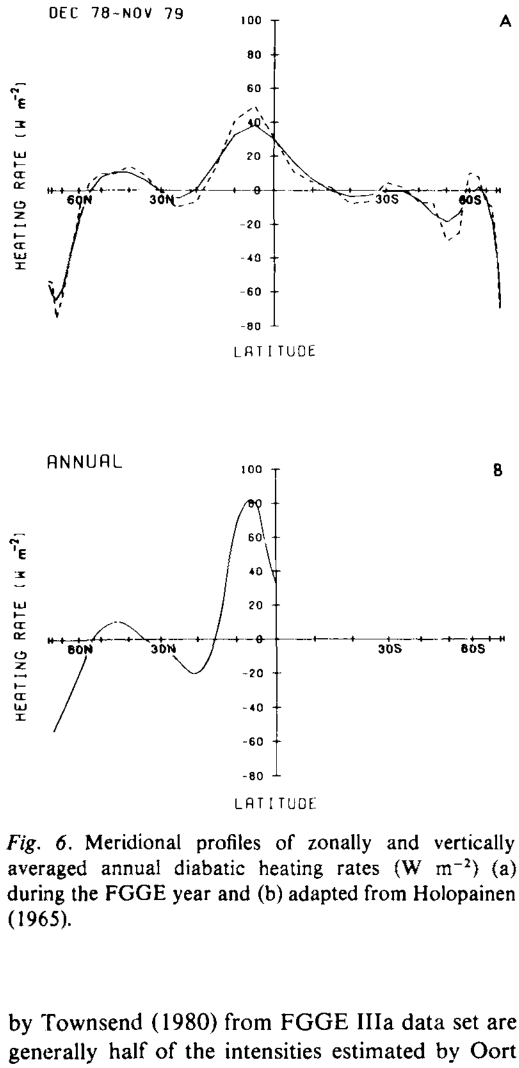

Fig. 6. Meridional profiles of zonally and vertically averaged annual diabatic heating rates (W m^{-2}) (a) during the FGGE year and (b) adapted from Holopainen (1965).

by Townsend (1980) from FGGE IIIa data set are generally half of the intensities estimated by Oort and Rasmusson (1970) with the exception of June–August when the strengths of the southern Hadley cell are comparable in both studies. Smaller meridional mass transport indicates weaker overturning, and therefore suggests less vertical mass transport within the ITCZ. This is consistent with the fact that the annual mean heating near 5–10° N in Fig. 6a is only about half of Holopainen's result (Fig. 6b). It may be a reflection of a weaker monsoon circulation during December 1978–February 1979 (Tanaka, 1981). A systematic bias may also exist in the NMC FGGE IIIa data set.

Several other calculations of diabatic heating, for example, Geller and Avery (1978), Hantel and Baader (1978) and Lau (1979), are also available in recent literature. In all three studies mentioned above the diabatic heating is deduced as a residual from some form of the thermodynamic equation. Lau (1979) based his calculation on twice-daily NMC analyses in isobaric coordinates for 11 winters from 1965–66 through 1975–76; his spatial domain included the Northern Hemisphere north of 20° N. The heating maxima for the east coasts of Asia and North America which extend across the oceans to the eastern portions of North Pacific and Atlantic near 40–60° N, respectively, are also observed by Lau. His results indicate diabatic heating is required over the southwestern United States and adjacent oceanic area to balance the strong divergence of heat fluxes by transient eddies. This feature is not observed in this study. For the most part, the magnitudes of heating and cooling are comparable between the two studies.

Both Geller and Avery (1978) and Hantel and Baader (1978) made use of the statistics from the General Circulation Library of the Massachusetts Institute of Technology (Oort and Rasmusson, 1971). The results in Geller and Avery consist of heating distributions of Northern Hemisphere for January, April, July and September at 900 mb and 500 mb, respectively. In general, the seasonal distribution and variation of diabatic heating in our study are more distinctly related to the land–ocean distribution than those in Geller and Avery. Aside from the difference in polar latitudes, several others are obvious. Cooling is indicated in the eastern oceans at about 40–60° N in January in Geller and Avery; whereas heating is shown in both Lau (1979) and the present study. Strong cooling over the eastern Pacific is contrasted with large heating near the dateline and 40° N in July and September; very intense cooling also exists over the middle Atlantic Ocean in July. None of these features is evident in our results.

Seasonal distributions of diabatic heating for the zonally averaged hemisphere north of 15° S are presented in Hantel and Baader (1978). Their meridional cross-sections are similar in structure to the results from our study except during spring and summer when heating is calculated for most of the troposphere in northern middle latitudes in their results whereas in our study cooling is indicated in the middle and upper troposphere. Except during summer, heating in the tropics and cooling in the subtropics are generally 2–3 times more intense in their results. However, the heating in the lower troposphere of middle latitudes in connection with baroclinic disturbances is more prominent in this study.

6. Summary and conclusion

The three-dimensional distribution of atmospheric diabatic heating has been estimated using the isentropic mass continuity equation with the FGGE Level IIIa data set generated by NMC. Because diabatic processes are uniquely related with vertical mass flux in the isentropic framework, the isentropic mass continuity equation proves to be a viable approach.

Seasonally and annually averaged diabatic heating distributions are presented. The results agree with other studies and climatological concepts, particularly in the tropics and Northern Hemisphere. Major features include heating in the intertropical convergence zone and the preferred region for deep moist convection in the western Pacific, heating along the east coasts of Asia and American continents in northern winter, and cooling in the subtropical anticyclonic areas as well as polar latitudes. The heating within the Asiatic monsoon is a persistent source of energy on the planetary scale and its position in the equatorial Pacific progresses with the seasons. Energy must be transported from this area to heat sink regions. Because the observational density in the IIIa analyses for the Southern Hemisphere is relatively sparse in comparison with the Northern Hemisphere, certain features in the mid and high latitudes are less certain.

The estimates presented in this study are not considered to be final. Fourier filtering and spatial smoothing have been used to obtain the large-scale features. Consequently some of the smaller-scale features are smoothed and less pronounced. The results are encouraging in that the features evident from NMC's IIIa analyses seem properly located along with reasonable values of heating. However, the question of assessing "noise" remains. Since FGGE level IIIb analyses contain more data from the special observing platforms, it will be especially interesting to compare the distribution of diabatic heating determined from the two sets of information. Such studies are important for the investigation of the thermal forcing of the atmosphere and provide useful information for modeling and studies of the planetary scale circulation.

7. Acknowledgements

This research was sponsored jointly by the Global Atmospheric Research Program of the National Science Foundation and the Special Research Programs Office of the National Oceanic and Atmospheric Administration under Grant ATM78-22384. Typing of the manuscript by Gail Turluck and Judy Mohr and preparation of the figures by Steve Hjortness are greatly appreciated.

REFERENCES

Atkinson, G. D. and Sadler, J. C. 1970. Mean-cloudiness and gradient-level-wind charts over the tropics. Tech. Report 215, Air Weather Service, USAF, Washington, D.C.

Bergman, K. H. 1979. A multivariate optimum interpolation analysis system of temperature and wind fields. *Mon. Wea. Rev. 107*, 1423–1444.

Budyko, M. I. 1963. *Atlas of the heat balance of the earth.* Moscow, Gidrometeoizdat., 69 pp.

Carlson, T. N. and Benjamin, S. G. 1980. Radiative heating rates for Saharan dust. *J. Atmos. Sci. 37*, 193–213.

Cox, S. K. and Ackerman, S. A. 1981. Radiative components of Saudi Arabian Peninsula heat low. ICSU/WMO GARP Condensed Papers and Meeting Report of International Conference on Early Results of FGGE and Large-Scale Aspects of its Monsoon Experiments (12–17 January 1981, Tallahassee, Florida), Geneva, 6.3–6.7.

Dutton, J. A. and Johnson, D. R. 1967. The theory of available potential energy and a variational approach to atmospheric energetics. *Adv. Geophys. 12*, 333–436.

Geller, M. A. and Avery, S. K. 1978. Northern Hemisphere distributions of diabatic heating in the troposphere derived from general circulation data. *Mon. Wea. Rev. 106*, 629–636.

Hantel, M. and Baader, H-R. 1978. Diabatic heating climatology of the zonal atmosphere. *J. Atmos. Sci. 35*, 1180–1189.

Hill, H. W. 1981. A synoptic case study using the FGGE buoy data of a typical low index regime in the western South Pacific Ocean. ICSU/WMO GARP Conference Proceedings on International Conference on Preliminary FGGE Data Analysis and Results (23–27 June 1980, Bergen, Norway), Geneva, 450–464.

Holloway, J. L. 1958. Smoothing and filtering of time series and space fields. *Adv. Geophys 4*, 351–389.

Holopainen, E. O. 1965. On the role of mean meridional circulations in the energy balance of the atmosphere. *Tellus 17*, 285–294.

Johnson, D. R. 1979. Systematic stratospheric–tropospheric exchange through quasi-horizontal transport processes within active baroclinic waves. WMO Symposium on Long-Range Transport of Pollutants and its Relation to General Circulation Including Stratospheric/Tropospheric Exchange Processes, October 1–5, 1979, Sofia, Bulgaria.

Johnson, D. R. 1980. A generalized transport equation for use with meteorological coordinate systems. *Mon. Wea. Rev. 108*, 733–745.

Johnson, D. R. and Downey, W. K. 1975. Azimuthally averaged transport and budget equations for storms: quasi-Lagrangian diagnostics 1. *Mon. Wea. Rev. 103*, 967–979.

Johnson, D. R. and Townsend, R. D. 1981. Diagnostics of the heat sources and sinks of the Asiatic monsoon and the thermally-forced planetary scale response. ICSU/WMO GARP Conference Proceedings on International Conference on Preliminary FGGE Data Analysis and Results (23–27 June 1980, Bergen, Norway), Geneva, 523–533.

Johnson, D. R., Townsend, R. D., Wei, M. Y. and Selin, R. D. 1981. The global structure of energy transport within thermally-forced planetary scale mass circulations. ICSU/WMO GARP Condensed Papers and Meeting Report of International Conference on Early Results of FGGE and Large-Scale Aspects of its Monsoon Experiments (12–17 January 1981, Tallahassee, Florida), Geneva, 3.27–3.34.

Lau, N.-C. 1979. The observed structure of tropospheric stationary waves and the local balances of vorticity and heat. *J. Atmos. Sci. 36*, 996–1016.

London, J. 1957. A study of the atmospheric heat balance. Final Report on contract AF19(122)-165, New York University, Department of Meteorology and Oceanography.

Lorenz, E. N. 1955. Available potential energy and the maintenance of the general circulation. *Tellus 7*, 157–167.

McPherson, R. D., Bergman, K. H., Kistler, R. E., Rasck, G. E. and Gordon, D. S. 1979. The NMC operational global data assimilation system. *Mon. Wea. Rev. 107*, 1445–1461.

Miller, D. B. and Feddes, R. G. 1971. Global atlas of relative cloud cover, 1967–70, based on photographic signals from meteorological satellites. U.S. Department of Commerce and United States Air Force, Washington, DC, 237 pp.

Newell, R. E., Vincent, D. G., Dopplick, T. G., Ferruzza, D. and Kidson, J. W. 1969. The energy balance of the global atmosphere. In: *The global circulation of the atmosphere*, G. A. Corby (ed.), Roy. Meteor. Soc., 42–90.

Newell, R. E., Kidson, J. W., Vincent, D. G. and Boer, G. J. 1974. *The general circulation of the tropical atmosphere and interactions with extratropical latitudes*, Vol. 2. The MIT Press, 371 pp.

Oort, A. H. and Rasmusson, E. M. 1970. On the annual variation of the monthly mean meridional circulation. *Mon. Wea. Rev. 98*, 423–442.

Oort, A. H. and Rasmusson, E. M. 1971. Atmospheric circulation statistics. NOAA Prof. Pap., No. 5, 323 pp.

Physick, W. L. 1981. Winter depression tracks and climatological jet streams in the Southern Hemisphere during the FGGE year. *Q. J. R. Meteorol. Soc. 107*, 883–898.

Streten, N. A. and Troup, A. J. 1973. A synoptic climatology of satellite observed cloud vortices over the Southern Hemisphere. *Q. J. R. Meteorol. Soc. 99*, 56–72.

Taljaard, J. J. 1967. Development, distribution and movement of cyclones and anticyclones in the Southern Hemisphere during IGY. *J. Appl. Meteorol. 6*, 973–987.

Tanaka, M. 1981. Interannual fluctuations of the tropical monsoon circulation over the greater WMONEX area. *J. Meteorol. Soc. Japan 59*, 825–831.

Townsend, R. D. 1980. A diagnostic study of the zonally-averaged global circulation in isentropic coordinates. Ph.D. thesis, University of Wisconsin, Madison, 221 pp.

Webster, P. J., Chou, L. and Lau, K. M. 1977. Mechanisms effecting the state of the planetary scale monsoon. *Pure Appl. Geophys. 115*, 1463–1491.

Year Book Australia, No. 65, 1981: Climate of Australia, 1981 Edition. Published by the Australian Government Publishing Service for the Bureau of Meteorology.